RADIATION RESEARCH **185**, 516–526 (2016)
0033-7587/16 $15.00

DOI: 10.1667/RR14261.1

Cerium Oxide Nanoparticles: A Potential Medical Countermeasure to Mitigate Radiation-Induced Lung Injury in CBA/J Mice

P-T. Xu,[a,1] B. W. Maidment 3rd,[b] V. Antonic,[a] I. L. Jackson,[a,1] S. Das,[d] A. Zodda,[a,1] X. Zhang,[a,1] S. Seal[c] and Z. Vujaskovic[a,1,2]

[a] *Department of Radiation Oncology, University of Maryland School of Medicine, Baltimore, Maryland 21201;* [b] *Department of Radiation Oncology, University of Virginia, Charlottesville, Virginia 22908; and* [c] *Advanced Materials Processing and Analysis Center, Nanoscience Technology Center, Materials Science and Engineering, University of Central Florida, Orlando, Florida 32826*

Xu, P-T., Maidment 3rd, B. W., Antonic, V., Jackson, I. L., Das, S., Zodda, A., Zhang, X., Seal, S. and Vujaskovic, Z. Cerium Oxide Nanoparticles: A Potential Medical Countermeasure to Mitigate Radiation-Induced Lung Injury in CBA/J Mice. *Radiat. Res.* 185, 516–526 (2016).

Cerium oxide nanoparticles (CNPs) have a unique surface regenerative property and can efficiently control reactive oxygen/nitrogen species. To determine whether treatment with CNPs can mitigate the delayed effects of lung injury after acute radiation exposure, CBA/J mice were exposed to 15 Gy whole-thorax radiation. The animals were either treated with nanoparticles, CNP-18 and CNP-ME, delivered by intraperitoneal injection twice weekly for 4 weeks starting 2 h postirradiation or received radiation treatment alone. At the study's end point of 160 days, 90% of the irradiated mice treated with high-dose (10 μ*M*) CNP-18 survived, compared to 10% of mice in the radiation-alone ($P < 0.0001$) and 30% in the low-dose (100 n*M*) CNP-18. Both low- and high-dose CNP-ME-treated irradiated mice showed increased survival rates of 40% compared to 10% in the radiation-alone group. Multiple lung functional parameters recorded by flow-ventilated whole-body plethysmography demonstrated that high-dose CNP-18 treatment had a significant radioprotective effect on lethal dose radiation-induced lung injury. Lung histology revealed a significant decrease ($P < 0.0001$) in structural damage and collagen deposition in mice treated with high-dose CNP-18 compared to the irradiated-alone mice. In addition, significant reductions in inflammatory response ($P < 0.01$) and vascular damage ($P < 0.01$) were observed in the high-dose CNP-18-treated group compared to irradiated-alone mice. Together, the findings from this preclinical efficacy study clearly demonstrate that CNPs have both clinically and histologically significant mitigating and protective effects on lethal dose radiation-induced lung injury.

INTRODUCTION

The lung tissues are among the most sensitive tissues to ionizing radiation (*1*). Respiratory failure due to radiation pneumonitis is a major cause of mortality after exposure to high-dose ionizing radiation (*2*). Exposure to radiation can result in excessive production of reactive oxygen species (ROS) and reactive nitrogen species (RNS) that can cause oxidative damage to DNA, lipids and proteins, resulting in cell injury or death (*3*). After irradiation, DNA damage leads to apoptosis of type I and II pneumocytes, and the proliferation of type II pneumocytes promotes the secretion of growth factors and proteases and degradation of the extracellular matrix to allow removal of dead cells by normal processes (*4*). Pulmonary irradiation also damages epithelial and endothelial cells, compromises vessel integrity, decreases microvessel density and lung perfusion and promotes hypoxia (*5*). While primary radiation-induced injury results in direct damage to cells, secondary effects are associated with increases in oxidative damage to DNA and ROS/RNS levels that can initiate and trigger a cascade of genetic and molecular reactions (*5–7*). Various free radical scavengers (e.g., amifostine, vitamin E, carotenes and melatonin) have been tested for their potential to mitigate the lethal dose radiation-induced cell and tissue damage with limited success (*8–12*).

Cerium oxide nanoparticles (CNPs) have a unique regenerative antioxidant property and can efficiently scavenge ROS/RNS (*13*). In recent *in vitro* and *in vivo* studies, specific CNP formulations were reported to demonstrate significant antioxidant potential, often with very little or no toxicity (*14*). Cerium can exist in either a fully oxidized (Ce^{4+}) or fully reduced (Ce^{3+}) state. At a molecular level, the Ce^{3+} state on the surface of CNPs is believed to confer SOD-mimetic properties, and the Ce^{4+} state is believed to confer catalase-mimetic properties (*13*). The unique autoregenerative property of CNPs makes them promising therapeutic reagents. Furthermore, their antioxidant effects may persist for a long period of time after a single dose (*15, 16*). CNPs have also shown a capacity to

[1] Previously affiliated with the Department of Radiation Oncology, Duke University Medical Center, Durham, NC 27710.
[2] Address for correspondence: UMSOM, Radiation Oncology, 685 W Baltimore St., MSTF7-00A, Baltimore, MD 27710; email: zvujaskovic@som.umaryland.edu.

protect biological tissues against radiation-induced damage (*17–19*), prevent laser-induced retinal damage (*15*), reduce chronic inflammation (*14*) and reduce oxidative stress-induced neuronal damage (*20*). CNPs protect the gastrointestinal epithelium from radiation-induced damage by reduction of ROS and upregulation of superoxide dismutase 2 (*21*). CNPs have also been shown to cause faster wound healing/closing by induction of cell proliferation, induction of angiogenesis and reduction the oxidative stress (*22, 23*). A recent *in vivo* study demonstrated that CNPs protect against radiation-induced pneumonitis in immunodeficient athymic nude mice (*24*).

In this pilot *in vivo* study, we evaluated the therapeutic efficacy of CNP-18 and CNP-ME (synthesized using two different methods) for preventing and mitigating radiation-induced lung injury and improving survival in CBA/J mice, a well-characterized murine model of lethal dose radiation-induced lung injury (*25, 26*). We also evaluated secondary end points including multiple pulmonary functional parameter changes, pathological structural damage and collagen deposition, inflammatory response and vascular damage.

MATERIALS AND METHODS

Cerium Oxide Nanoparticle Synthesis and Characterization

The cerium oxide nanoparticles were synthesized using two different methods: microemulsion (CNP-ME) (*27*) and wet chemical preparation (CNP-18) (*28*). Cerium nitrate hexa-hydrate of 99.999% purity was used for both preparations. The microemulsion process consisted of surfactant sodium bis (2-ethylhexyl) sulfosuccinate (AOT), toluene and water. Aqueous cerium nitrate (0.1 mol/l) was mixed with 50 ml toluene-AOT mixture, and then 5 ml 30% H_2O_2 was added to the mixture and stirred for 2 h. The mixture was then allowed to separate into two layers overnight; the toluene layer was collected and 10 ml 30% NH_4OH was added to precipitate the CNPs. The CNPs were then washed thoroughly using acetone and water to remove any residual surfactant and suspended in distilled water (ddH_2O). CNP-18 was synthesized by a simple wet chemical method that has been described previously (*14*). Briefly, cerium nitrate was dissolved in 50 ml of ddH_2O (final concentration 5 m*M*) and then stoichiometric H_2O_2 was added to the solution. Lastly, acidic pH (~4) was adjusted to maintain a good suspension. Size and morphology of the particles were analyzed using high-resolution transmission microscopy (HRTEM) (Tecnai™ F30; FEI™; Hillsboro, OR). Crystallinity of the nanoparticles was determined from the selected area electron diffraction (SAED) pattern. Surface charge and hydrodynamic radius were assayed using a dynamic light scattering instrument (Malvern Instruments, Malvern, UK). Surface chemistry of CNPs was determined using X-ray photoelectron spectroscopy as described elsewhere (*29*).

Animals and Irradiation

Female CBA/J mice (8–10 weeks of age, 21–25 g) were purchased from Jackson Laboratory (Bar Harbor, ME). All mice were housed 5 per cage at the Duke Genome Science Research Building II (GSRBII), a barrier facility, and provided food and water *ad libitum*. All experiments were performed with prior approval from the Duke University Institutional Animal Care and Use Committee (IACUC). After a 2–3 weeks of acclimation to the facility, mice were anesthetized by intraperitoneal (IP) injection of 100 mg/kg ketamine and 10 mg/kg xylazine and were 15 Gy whole-thorax irradiated at a dose rate of 69 cGy min^{-1} (320 kVp, 10 mA and HVL = 1.00 mm Cu) (Precision X-ray Inc., North Branford, CT). Animals were irradiated in groups of 10. After irradiation, mice were kept on heating blankets to help maintain normal body temperature until fully awake and mobile. Prior to animal irradiation, technical validation, including 2D field uniformity and dose-rate linearity, were determined using Gafchromic™ film and metal oxide semiconductor field effect transistor (MOSFET) detectors as described previously by McGurk *et al*. (*30*). Entrance and target tissue dose rates were determined using tissue-equivalent mouse phantoms and implanted detectors *in vivo*.

Cerium Oxide Nanoparticles Dosing

Female CBA/J mice were randomized into 8 groups of 10 mice, as follows:

1. radiation alone [whole-thorax lung irradiation (WTLI; 15 Gy) + saline injection];
2. radiation + CNP-18-L (15 Gy WTLI + 100 n*M* CNP-18 treated, low dose = 0.00007 mg/kg);
3. radiation + CNP-18-H (15 Gy WTLI + 10 μ*M* CNP-18 treated, high dose = 0.007 mg/kg);
4. radiation + CNP-ME-L (15 Gy WTLI + 100 n*M* CNP-ME treated, low dose = 0.00007 mg/kg);
5. radiation + CNP-ME-H (15 Gy WTLI + 10 μ*M* CNP-ME treated, high dose = 0.007 mg/kg);
6. CNP-18 alone [10 μ*M* CNP-18 injection (control)];
7. CNP-ME alone [10 μ*M* CNP-ME injection (control)]; and
8. Sham irradiation [saline injection alone normal (control)].

Nanoparticles and saline were delivered by IP injection twice a week (Monday and Thursday) for 4 weeks starting 2 h postirradiation.

Survival Analysis

Mice were closely monitored daily for signs of respiratory distress over the first 22 weeks postirradiation, including hypomotility, hunchback posture and tachypnea. Animals exhibiting more than 20–25% body weight loss, lethargy, hunchback posture, ruffled fur were euthanized. Mice with extreme respiratory distress were euthanized by administering barbiturate overdose (>250 mg/kg) in accordance with Duke Veterinary guidelines, then necropsied with measurement of lung tissue mass and pleural fluid content. All surviving mice were euthanized at a predetermined study end point of 160 days.

Functional Assessment of Lung Damage Using Flow Whole-Body Plethysmography

Unrestrained bias-flow ventilated whole-body plethysmography (WBP; Buxco Electronics, Wilmington, NC), which is a noninvasive method, was used to monitor longitudinal pulmonary function of irradiated CBA/J mice treated with CNP-18 or CNP-ME and sham-irradiated control mice every two weeks after irradiation. Mice were placed unrestrained and unsedated in cylindrical plethysmography chambers and allowed to acclimate to the chambers for ~5 min and to show normal exploratory behavior, and then respiratory functional parameters were recorded for 15 min. All respiratory parameters were generated and collected simultaneously by the WBP instrument. All parameters were recorded and exported automatically without manipulation to demonstrate longitudinal pulmonary functional status of individual irradiated mice. Multiple lung function parameters include breathing rate (F), tidal volume (TV), minute volume (MV), enhanced pause (Penh), pause (PAU), inspiratory time (Ti), peak inspiratory flow (PIF), expiratory time (Te), peak expiratory flow (PEF), relaxation time (Tr), tidal midexpiratory flow (EF50) and total expiratory time (Rpef), which is the ratio of time from initiation of expiration to when peak expiratory flow is reached.

TABLE 1
Physicochemical Properties of Cerium Oxide Nanoparticles (CeO_2) Prepared by Wet Chemical (CNP-18) and Microemulsion Process (CNP-ME)

Nanoparticles	Morphology	Crystalline property	Size (nm; HRTEM)	Hydrodynamic size (nm)	ZP (mV)	Possible surface contamination	Surface Ce^{3+}/Ce^{4+} ratio
CNP-18	Round/irregular	Crystalline fluorite structure	3–5	38.11 ± 5.57	19.1 ± 1.4	-	1.26
CNP-ME	Round/irregular	Crystalline fluorite structure	3–5	91.93 ± 13.45	–20.4 ± 1.47	AOT	0.45

Gross Morphology and Histopathology

Mice were euthanized for assessment of tissue lung mass (a marker of edema and congestion) and pleural effusions at the time of imminent mortality and all surviving mice were euthanized 160 days postirradiation. After euthanization, a bilateral thoracotomy was performed and the whole lungs and heart were excised and rinsed briefly in cold phosphate-buffered saline, after which wet lung weight was recorded. The right lung and heart were frozen in liquid nitrogen and stored at −80°C. The left lung was fixed using formalin and evaluated for gross morphology and degree of fibrosis. Fixed lungs sectioned at 5 μm thickness were stained with hematoxylin and eosin (H&E) for assessment of inflammatory cells, alveolar capillary distension or congestion, presence of hyaline membranes and alveolar wall thickness. Masson's trichrome stain was used to assess the degree of fibrosis. Quantitative assessment of the degree of interstitial fibrosis was determined using a numerical scale of 0–8 based on the Ashcroft scoring method (*31*) with standardized modification as described by Hübner *et al*. (*32*).

Statistical Analysis

Data are expressed as the mean ± standard error of the mean (SEM). The effects of cerium oxide nanoparticles on radiation-induced lung damage were analyzed by paired sample *t* tests within each group. One-way analysis of variance (ANOVA) with multiple comparisons test was performed to determine the statistical significance of differences in lung weight among groups. Intra-group comparisons were performed using one-way ANOVA with repeated measures at each time.

RESULTS

Nanoparticle Characterization

Cerium oxide nanoparticles used in this study were synthesized, maintaining a sterile environment. Since the physicochemical properties of synthesized CNPs play a critical role in determining cell–nanoparticle interactions as well as ROS/RNS scavenging capabilities, these parameters were analyzed thoroughly for both CNP-18 and CNP-ME (see Table 1 for results). HRTEM images show CNP-18 and CNP-ME were 3–5 nm crystalline particles with round-to-irregular morphology (Fig. 1). However, the hydrodynamic radiuses for CNP-18 and CNP-ME were observed to be ~38 and 91 nm, respectively. The increase in size indicates the formation of loose agglomerate in an aqueous environment. The measured surface charge was indicated as positive for CNP-18 (19.1 mV) and negative for CNP-ME (−20.4 mV). As mentioned earlier, surface oxidation ratio regulates the ROS/RNS scavenging property, with higher Ce^{3+}/Ce^{4+} ratio particles reported to have higher superoxide dismutase mimetic activity. Conversely, lower Ce^{3+}/Ce^{4+} ratio particles are more catalase mimetic (*13*). Interestingly, higher surface Ce^{3+}/Ce^{4+} ratio was observed in CNP-18 (1.26) compared to CNP-ME (0.45). These two

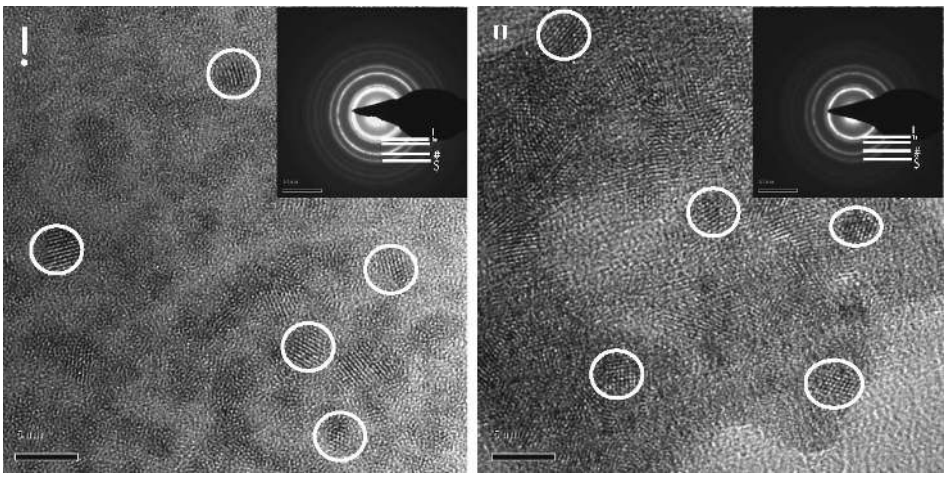

FIG. 1. High-resolution transmission microscopy image of CNPs. Panel A: CNP-18 synthesized using wet chemical method [inset: selected area electron (SAED) pattern]. Panel B: CNP-ME synthesized using microemulsion process (inset: SAED pattern). Inset key: A, B, C and D represent 111, 200, 220 and 311crystal lattice planes, respectively, of CNP fluorite lattice structure. Scale bar = 5 nm.

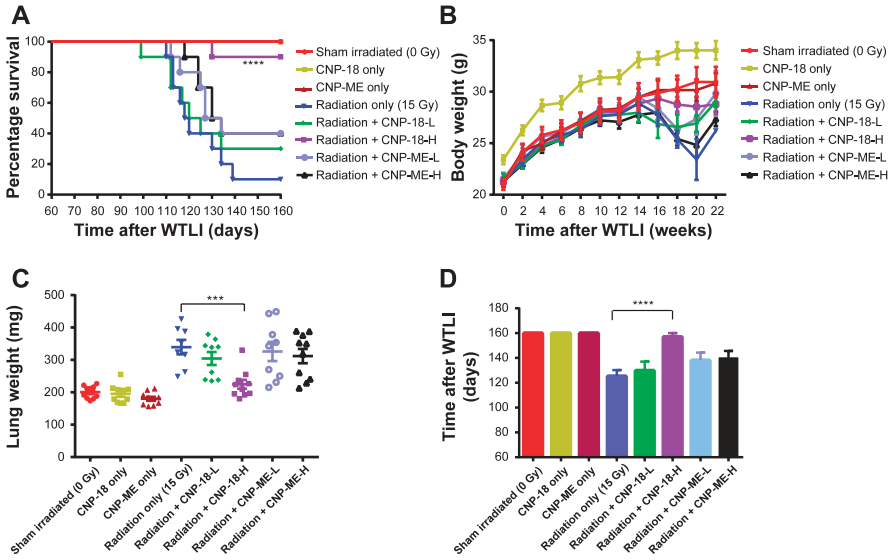

FIG. 2. Mitigating effects of cerium oxide nanoparticles (CNP-18 and CNP-ME) on radiation-induced lung injury in CBA/J mice. Panel A: Kaplan-Meier survival curves for 160 days. The radiation + CNP-18-H mice demonstrated significant improvement in the survival rate (90%, 9/10), compared to the radiation-alone group (10%, 1/10; $P < 0.0001$). Both the radiation + CNP-ME-L and radiation + CNP-ME-H groups showed increased survival rates (40%, 4/10). Panel B: Body weight. All irradiated mice except the radiation + CNP-18-H group had obvious body weight loss starting from 16 weeks after WTLI. Panel C: Wet lung weight. All irradiated groups except the radiation + CNP-18-H group had significantly higher lung weight compared to the sham-irradiated control. The radiation + CNP-18-H group had a significantly lower lung weight than the radiation-alone group ($P < 0.001$). Panel D: Mean survival days. The radiation + CNP-18-H mice had a significantly longer survival time than the radiation-alone mice ($P < 0.0001$). Data shown are the mean ± SEM. ****$P < 0.0001$, ***$P < 0.001$, radiation + CNP-18-H vs. radiation alone.

particles were tested for radiation mitigation activity in our *in vivo* model of radiation-induced lung injury.

Survival

To evaluate the radiation mitigation activity of CNPs, CBA/J mice were 15 Gy WTLI in the presence or absence of twice weekly IP injections of CNPs starting 2 h postirradiation for a duration of four weeks (total 8 injections). Our results show (Fig. 2A) that both CNP-18 and CNP-ME nanoparticles are well tolerated by CBA/J mice. The survival rate of irradiated mice was significantly increased (90%, 9/10, $P < 0.0001$) in mice treated with high-dose (10 μM) CNP-18 compared to the radiation-alone group (10%, 1/10). The survival rate of radiation + CNP-18-L mice (30%, 3/10) was slightly higher than the radiation-alone control, which lacked statistical significance ($P = 0.60$). Both low- and high-dose CNP-ME-treated irradiated mice showed an increased survival rate (40%, 4/10), which was marginally significant compared to radiation-alone mice ($P = 0.125$, radiation + CNP-ME-L vs. radiation alone; $P = 0.065$, radiation + CNP-ME-H vs. radiation alone).

Body Weight

The mouse body weight was measured before irradiation and then biweekly after irradiation through 22 weeks, the time point of euthanization (Fig. 2B). Assessment of body weight changes over time was intended to serve as an indication of systemic toxicity of radiation-induced lung injury. The radiation-alone mice had a significantly lower body weight than either the sham-irradiated control or CNPs-alone treated mice from weeks 14–22 (Fig. 2B). A larger number of radiation-alone mice (6/10) had more than 15% body weight loss from recorded peak body weight from weeks 16–20 (Fig. 2B, Table 2). The radiation + CNP-18-H mice did not experience significant weight loss over the duration of the study. The majority of the radiation + CNP-18-H mice (7/10) had less than 5% body weight loss compared to the radiation-alone mice (1/10) and radiation + CNP-18-L mice (2/10) (Fig. 2B, Table 2).

Wet Lung Weight

Wet lung weights are recorded as a marker of pulmonary edema and congestion associated with pneumonitis at the time of necropsy. Significantly lower wet lung weights (224.7 ± 13.8 mg) were observed in the radiation + CNP-18-H mice compared to the radiation-alone mice (339.5 ± 22.4 mg) ($P < 0.001$; Table 2, Fig. 2C). There was no significant difference in average lung weights between the radiation + CNP-18-H mice and sham-irradiated control mice (compared 224.7 mg vs. 200.5 mg; Table 2). We did not observe a significant difference in lung weights in radiation + CNP-18-L or both low- and high-dose CNP-ME irradiated mice compared to the radiation-alone mice (Fig.

TABLE 2
Clinical Manifestations and Histopathology of Irradiated Animals Treated or Untreated with Cerium Oxide Nanoparticles

	Sham irradiation (0 Gy)			Whole-thorax irradiation (15 Gy)				
	Saline	CNP-18 (10 m*M*)	CNP-ME (10 m*M*)	Radiation alone (saline)	Radiation + CNP-18-L (100 n*M*)	Radiation + CCNP-18-H (10 m*M*)	Radiation + CCNP-ME-L (100 n*M*)	Radiation + CCNP-ME-H (10 m*M*)
Body weight loss								
0–5%	0	0	1/10	1/10	2/10	7/10	4/10	4/10
5–15%	0	0	0	3/10	2/10	2/10	1/10	0/10
>15%	0	0	0	6/10	6/10	1/10	5/10	6/10
Lethality (%)	0	0	0	90%	70%	10%	60%	60%
Decedents/total	0/10	0/10	0/10	9/10	7/10	1/10	6/10	6/10
Median survival (day)	160	160	160	119	122.5	160	130.5	132
Mean survival ± SEM	160 ± 0	160 ± 0	160 ± 0	125.3 ± 4.9	129.9 ± 7.2	157 ± 3.0	138.1 ± 6.3	140 ± 5.6
25–75th percentile	160–160	160–160	160–160	113–135.3	112–160	160–160	122.8–160	124–160
Lower 95% CI of mean	160	160	160	114.1	113.7	150.2	123.9	127.3
Upper 95% CI of mean	160	160	160	136.5	146.1	163.8	152.3	152.7
Lung weight ± SEM (mg)	200.5 ± 6.1	195.1 ± 8.9	180 ± 6.1	339.5 ± 22.4	304.4 ± 19.9	224.7 ± 13.8	325.9 ± 29.5	311.9 ± 21.9
Fibrosis score ± SEM	0	0	0	4.85 ± 0.11	5.28 ± 0.10	3.05 ± 0.06	5.17 ± 0.18	4.48 ± 0.25
Inflammation score ± SEM	0	0	0	3.56 ± 0.06	3.44 ± 0.12	2.30 ± 0.15	3.67 ± 0.14	3.36 ± 0.15
Vascular damage ± SEM	0	0	0	2.69 ± 0.19	3.00 ± 0.16	1.73 ± 0.14	2.97 ± 0.09	2.94 ± 0.03

2C, Table 2). Both CNP-18 and CNP-ME-treated control mice had similar lung weights compared with sham-irradiated mice (Table 2), indicating that the CBA/J mice tolerated the high dosing of nanoparticles used in this study (Fig. 2C).

Median Survival Time

The mean survival time of radiation + CNP-18-H mice was significantly increased (157 ± 3.0 days) compared to radiation-alone mice (125 ± 4.9 days) ($P < 0.0001$; Fig. 2D, Table 2). Both low- and high-dose CNP-ME irradiated mice showed an improvement of mean survival (138 ± 6.3 and 140 ± 5.6 days, respectively) compared to the radiation-alone group (125 ± 4.9 days) (Fig. 2D, Table 2).

Respiratory Functional Assessment

Noninvasive bias-flow-ventilated whole-body plethysmography (Buxco, Wilmington, NC) was used to quantitatively analyze longitudinal respiratory function in individual irradiated CBA/J mice with and without CNP treatment. As shown in Figs. 3A–D and 4A–B, multiple lung function parameters demonstrated significant variation starting from week 14 after WTLI, reaching peak levels at week 16 and 18, which corresponded to the highest lethality weeks and the most severe bronchoconstriction. At week 20 and 22, due to many deaths of moribund animals, the recorded respiratory parameters decreased in the mean among groups compared to week 16 and 18, which recorded the surviving animals and thus, those in less respiratory distress. Table 3 summarizes the numbers of mice in each group (n = 10) that were recorded with significant percentage changes of respiratory parameters at week 16 and 18 compared to the corresponding sham-irradiated control parameters.

In our experiments, the respiratory rates in CBA/J mice range from 350 to 425 breaths per minute in healthy sham-irradiated control mice (Fig. 3A, Table 3). Significantly higher breathing rates were measured in radiation-alone mice from weeks 16–22 compared to sham-irradiated control mice, CNP-18- and CNP-ME-alone treated mice. The radiation + CNP-18-H-treated mice demonstrated significantly lower breathing rates with only 30% (3/10) of the treated mice showing a more than 10% breathing rate increase compared with 100% (10/10) radiation-alone mice showing a more than 10% breathing rate increase (Table 3) at week18 after WTLI. The radiation + CNP-18-L and both high- and low-dose CNP-ME treatments failed to correct radiation-induced high breathing rates from weeks 16–22 with 80% (8/10), 60% (6/10) and 70% (7/10) of the treated mice showing more than 10% breathing rate increase, respectively (Fig. 3A, Table 3).

Tidal volume reflects the amount of air exchanged per breath in ml. The sham-irradiated and CNPs-alone control mice showed a steady increase in tidal volume from weeks 2–22. Obviously lower tidal volumes were measured in radiation-alone mice from weeks 16–22. The radiation + CNP-18-H-treated mice demonstrated similar steady tidal volume value increases during the entire course observation. The radiation + CNP-18-L-treated mice and both high- and low-dose CNP-ME-treated mice showed similarly reduced tidal volume levels compared with radiation-alone mice (Fig. 3B, Table 3). The inspiratory time is measured in seconds and indicates the period from initiation of inspiration to end of inspiration.

There were no obvious differences in the inspiratory time value in sham-irradiated and CNPs-alone control mice in the entire 22 weeks of observation. All the irradiated mice except the radiation + CNP-18-H mice showed slight reduction in the inspiratory time value from weeks 16–22

(Fig. 3C). The radiation + CNP-18-H mice demonstrated similar inspiratory time value to sham-irradiated control mice (Fig. 3C).

The tidal midexpiratory flow (EF50) is defined as the tidal flow (ml/s) at the midpoint (50%) of expiratory tidal volume (*33*). During airway constriction, the main changes in the tidal flow signal occur during the midexpiratory phase. EF50 is used as a measure of physiologically meaningful and noninvasive parameter of bronchoconstriction for mice and rats (*34, 35*). The radiation + CNP-18-H-treated mice showed similar EF50 value compared with those of sham-irradiated and CNPs-alone control mice with slight increases at week 18 (Fig. 3D) and only 2 of 10 mice had a 25% increase in EF50 value (Table 3). The radiation-alone and radiation + CNP-18-L or CNP-ME-treated mice showed significant elevation in EF50 value compared with sham-irradiated control, particularly for week 18 (Table 3).

Minute volume indicates the volume of air exchange in units of ml/min. All irradiated and CNPs-alone control mice showed no significant difference from sham-irradiated control mice with a steady increase in minute volume from weeks 2–22. The irradiated mice may make an effort to compensate for reduced tidal volume by elevating their respiratory rate, suggesting that they are attempting to maintain minute volume (Fig. 3E, Table 3).

The peak inspiratory flow is measured in ml/s and indicates the maximum inspiratory flow rate. There were steady and continuous increases in peak inspiratory flow volume in sham-irradiated and CNPs-alone control mice (Fig. 4F). There was no significant difference in peak inspiratory flow value in the radiation + CNP-18-H mice (Table 3). The peak inspiratory flow values in radiation-alone mice, radiation + CNP-18-L and CNP-ME-treated irradiated mice showed a slight reduction from weeks 18–20 compared with sham-irradiated control mice.

Expiratory time is the time in seconds from the initiation of expiration to end expiration. The expiratory time of the radiation-alone mice was significantly decreased as compared to sham-irradiated control and CNPs-alone injected mice 16–22 weeks after WTLI (Fig. 3G). The radiation + CNP-18-H mice showed no obvious decrease in expiratory time value from weeks 16–22 compared with those of sham-irradiated control mice (Fig. 3G). In contrast, the radiation-alone mice, radiation + CNP-18-L or CNP-ME-treated irradiated mice showed similar reductions in expiratory time value compared with sham-irradiated control from weeks 16–22, among which a larger percentage of mice (70–90%) showed more than 25% expiratory time value reduction (Fig. 3G, Table 3).

The enhanced pause is a dimensionless composite value = (PEF/PIF) × (Te/Tr – 1). Increases in enhanced pause reflect elevations in expiratory time and peak expiratory flow and decreases in relaxation time and peak inspiratory flow (*36*). The enhanced pause of the sham-irradiated and CNPs-alone control mice were not altered at any time point of the experiment (Fig. 4H). The radiation-alone mice showed significant elevation from weeks 16–20 and 80% (8/10) of the radiation-alone mice showed more than 100% increase in enhanced pause (Table 3). Interestingly, the radiation + CNP-18-H mice showed a slightly higher enhanced pause (Fig. 4H) than sham-irradiated control mice from weeks 16–22, and only two mice (2/10) had more than 100% increase in enhanced pause value (Table 3). This result suggests high-dose CNP-18 treatment can correct radiation-induced elevated enhanced pause and decrease pulmonary distress. In contrast, radiation + CNP-18-L- and CNP-ME-treated irradiated mice showed significant increases in enhanced pause from 14 weeks postirradiation and maintained higher levels during weeks 16–20.

Relaxation time is defined as time to expire 65% of the inhaled volume (*36, 37*). The relaxation time of sham-irradiated and CNPs-alone control mice were not significantly altered in the entire period of experiment. All of 10 radiation-alone mice showed a 30% decrease of relaxation time value during weeks 16–22, with peak value reduction at week 18 (Fig. 3I, Table 3). There were similar levels of relaxation time value reduction in radiation + CNP-18-L- and CNP-ME-treated irradiated mice compared to radiation-alone mice. The radiation + CNP-18-H mice had a slight decrease in relaxation time value compared to sham-irradiated control mice from weeks 18–22, with only 3 of 10 mice showing more than 30% decrease in relaxation time value (Table 3).

Peak expiratory flow is the maximum flow rate during expiration, measured in ml/s. In general, there was a steady increase in the peak expiratory flow value over the entire experiment period. All irradiated mice except the radiation + CNP-18-H group had a slightly higher peak expiratory flow value compared to the sham-irradiated mice at week 18 (Fig. 3J) and 3 of 10 mice in radiation + CNP-18-H group showed more than 10% increase in peak expiratory flow value compared to 9 of 10 mice in the radiation-alone group at week 18 (Table 3).

The pause is designed to measure the ratio of the average flow during the first 65% of the expiration versus the average flow during the last 35% of the expiration (*36*). Pause is expressed as Te/Tr – 1. Increasing resistance increases the average height of early expiration. The distribution patterns of pause value changes in different experiment groups are similar to the observed changes of enhanced pause between groups (Fig. 3K).

Total expiratory time is a unitless measurement based on the WBP waveform that measures the ratio of time from initiation of expiration to total expiratory time (when peak expiratory flow is reached). The total expiratory time value will decrease under severe bronchoconstriction (*36*). The total expiratory time values of sham-irradiated and CNPs-alone-treated mice were not significantly altered during the experiment, showing only a slight reduction from weeks 20 and 22. The radiation-alone mice showed a significant decrease in total expiratory time values from weeks 16–22, and a larger percentage (70%, 7/10) of the mice had more

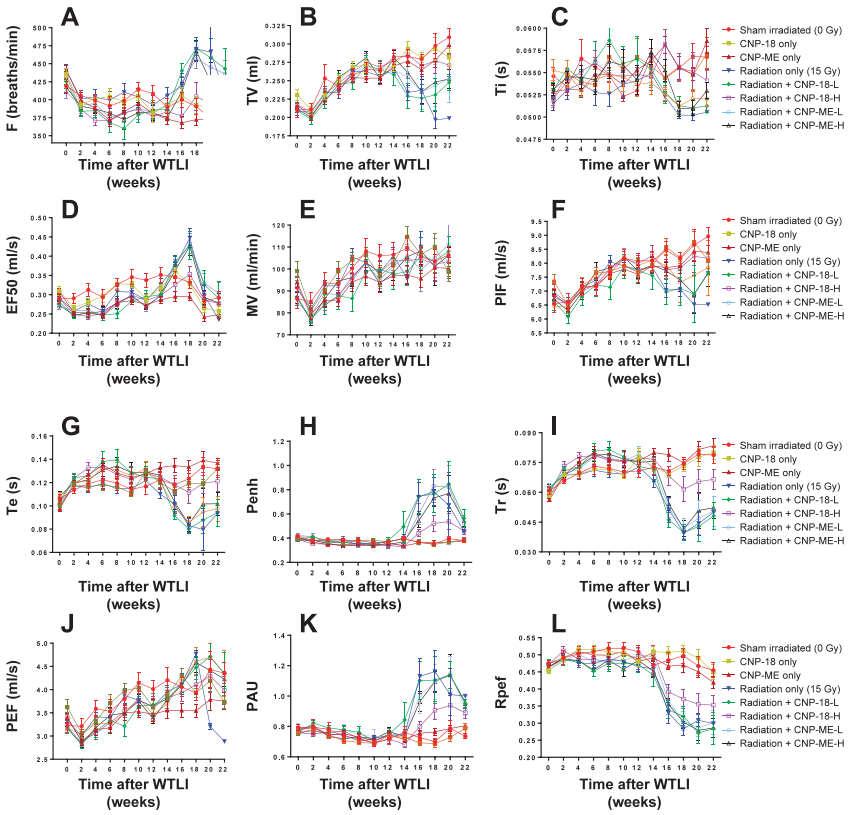

FIG. 3. Panel A: Breathing rates (F) were recorded biweekly from week 0–22. Breathing rates measured at weeks 16–22 in the following groups were significantly higher compared to: radiation alone; radiation + CNP-18-L; radiation + CNP-ME-L; and radiation + CNP-ME-H vs. sham-irradiated control mice. The radiation + CNP-18-H mice exhibited breathing rates significantly lower than those of the radiation-alone group from weeks 16–20, similar to those of the sham-irradiated control mice. Panel B: Tidal volume (TV) reflects the amount of air exchange per breath in ml. Sham-irradiated control mice and CNP-alone-treated mice showed a steady increase in tidal volume from week 0–22. Significantly lower tidal volume value was measured in radiation-alone mice from weeks 16–22 compared to sham-irradiated control mice. The radiation + CNP-18-H mice demonstrated a steady tidal volume increase similar to the sham-irradiated controls. Both high- and low-dose CNP-ME and low-dose CNP-18 treatment did not correct radiation-reduced tidal volume found in irradiated mice. Panel C: Inspiratory time (Ti) is measured in seconds and indicates the period from initiation to end of inspiration. All irradiated mice except the radiation + CNP-18-H group showed obvious reduction in the : inspiratory time value from weeks 16–22. The radiation + CNP-18-H mice had a Ti value similar to the sham-irradiated control mice. Panel D: The EF50 value is defined as the tidal flow (ml/s) at the midpoint (50%) of expiratory tidal volume. The radiation + CNP-18-H mice had an EF50 value similar to that of the sham-irradiated control mice (with slight increases at week 18). The radiation-alone mice and low-dose CNP-18- or CNP-ME-treated, irradiated mice showed a significantly elevated EF50 value compared to the sham-irradiated control group, particularly for week 18. Panel E: Minute volume (MV) is the volume (ml) of air exchange in minutes, indicated as ml/min. All irradiated and CNP-alone control mice showed no significant difference from the sham-irradiated control mice, with a steady increase in minute volume from weeks 2–22. Panel F: Peak inspiratory flow (PIF) is measured in ml/s and indicates the maximum inspiratory flow rate. There was a steady increase in peak inspiratory flow value in the sham-irradiated and CNP-alone control mice. There was no significant difference in peak inspiratory flow value in radiation + CNP-18-H mice compared to sham-irradiated control mice. The peak inspiratory flow values in radiation-alone mice, radiation + CNP-18-L- and CNP-ME-treated irradiated mice exhibited obvious reduction from weeks 18–22 compared to the sham-irradiated control group. Panel G: Expiratory time (Te) is the time in seconds from initiation to end of expiration. The radiation + CNP-18-H mice showed a expiratory time value similar to those of the sham-irradiated and CNP-alone control mice. The radiation-alone mice and radiation + CNP-18-L or CNP-ME-treated irradiated mice showed obvious reduction in expiratory time value compared to the sham-irradiated control group from weeks 16–22. Panel H: Enhanced pause (Penh) is a dimensionless composite value derived from: (PEF/PIF) × (Te/Tr – 1). All irradiated mice except the radiation + CNP-18-H group showed significant enhanced pause elevation from weeks 16–20 compared to the sham-irradiated control group. The radiation + CNP-18-H mice had a slight increase in enhanced pause compared to the sham-irradiated control mice from weeks 16–22. Panel I: Relaxation time (Tr) is defined as the amount of time needed to expire 65% of the inhaled volume. All irradiated mice except the radiation + CNP-18-H group showed similar levels of relaxation time value reduction compared to the sham-irradiated mice from weeks 16–22. The radiation + CNP-18-H mice had a slight decrease in relaxation time value compared to the sham-irradiated control mice from weeks 16–22. Panel J: Peak expiratory flow (PEF) is the maximum flow rate (ml/s) during expiration. There were no obvious significant differences among all control

TABLE 3
Number of Mice per Group with Respiratory Function Changes at or above the Indicated Percentages Compared to Sham-Irradiated Controls

		Sham irradiation (0 Gy)			Whole-thorax irradiation (15 Gy)				
Respiratory parameters	Percentage change vs. sham irradiation	Saline	CNP-18 (10 μ*M*)	CNP-ME (10 μ*M*)	Radiation alone (saline)	Radiation + CNP-18-L (100 n*M*)	Radiation + CNP-18-H (10 μ*M*)	Radiation + CNP-ME-L (100 n*M*)	Radiation + CNP-ME-H (10 μ*M*)
Breathing rate	10% increase	0	0	0	10	8	3	6	7
Tidal midexpiratory flow (EF50)	25% increase	0	0	0	8	7	2	4	5
Tidal volume	15% decrease	0	1	0	8	7	3	5	5
Minute volume	10% decrease	0	1	3	0	5	1	3	2
Inspiratory time	5% decrease	0	0	0	10	6	2	7	6
Peak inspiratory flow	15% decrease	0	0	0	5	7	2	5	4
Expiratory time	25% decrease	0	0	0	9	9	3	8	7
Peak expiratory flow	10% increase	0	0	0	9	7	3	4	6
Enhance pause	100% increase	0	0	0	8	6	2	5	5
Pause	40% increase	0	0	0	9	7	3	6	6
Relaxation time	30% decrease	0	0	0	10	9	3	7	7
Ratio of expiratory time → peak expiratory flow: total expiratory time	40% decrease	0	0	0	7	6	2	5	5

than 40% total expiratory time value decreases. The radiation + CNP-18-H mice had a noticeably smaller magnitude decrease in total expiratory time value compared to radiation-alone mice from weeks 16–22, with only 2 of 10 mice showing a more than 40% total expiratory time value reduction (Fig. 3L, Table 3). There were similar levels of total expiratory time reduction in radiation + CNP-18-L- and CNP-ME-treated irradiated mice compared with radiation-alone mice.

Histopathology

To determine the degree of radiation-induced pneumonitis and fibrosis, the left lungs were harvested and processed for H&E and Masson's trichrome staining. Pulmonary fibrosis was quantified using standardized scores on a scale of 0–8 as described by Hübner *et al*. (*32*) and Ashcroft *et al*. (*31*). Both sham-irradiated normal (Fig. 4A) and CNP-18-alone-treated control (Fig. 4D) lung sections had normal pulmonary architecture. Histology analyses of the lungs of the radiation-alone mice indicate evidence of severe radiation-induced pneumonitis (Fig. 4B and E). In contrast, the lungs of radiation + CNP-18-H mice showed significantly less damage with respect to inflammation and greater overall volume of normal lung, indicating that CNP-18 given at a high dose can preserve normal pulmonary architecture (Fig. 4C and F). The lungs of radiation + CNP-18-H mice displayed significantly less fibrosis (fibrosis grade = 3.05 ± 0.06) than the radiation-alone mice (4.85 ± 0.11, $P < 0.0001$) at 160 days (22 weeks) after WTLI (Fig. 5A, Table 2). At the same time point, no significant difference was found between radiation + CNP-18-L (5.28 ± 0.10) and radiation-alone (4.85 ± 0.11) mice (Fig. 5A, Table 2). No significant protection was observed in the irradiated mice treated with high- or low-dose CNP-ME (Table 2). In addition, significant reductions of inflammation ($P < 0.01$) and vascular damage ($P < 0.01$) were observed in the radiation + CNP-18-H group compared to the radiation-alone mice (Fig. 5B and C). The lungs from radiation-alone mice showed severe pneumonitis with extensive macrophage infiltration (Figs. 5B and 4B) with inflammation score of 3.56 ± 0.06, whereas the lungs from radiation + CNP-18-H mice showed much less pneumonitis

←
and irradiated groups, with a steady increase in peak expiratory flow value over the duration of the experiment. In the radiation-alone group, only 2 mice survived 20 weeks and 1 mouse survived 22 weeks after WTLI, with all three showing a significant reduction in peak expiratory flow value. Each value is the mean ± SEM. Panel K: Pause (PAU) is expressed as Te/Tr – 1, which represents the ratio of the average heights of early expiration (Tr) to late expiration (Te – Tr). There were similar distribution patterns of pause value changes to those of enhanced pause in different experiment groups. Panel L: Total expiratory time (Rpef) is a unitless measurement based on the WBP waveform that measures the ratio of time from initiation of expiration to total expiratory time (when peak expiratory flow is reached). The total expiratory time values of sham-irradiated and CNPs-alone control mice were not significantly altered during the entire period of experiment. All irradiated groups except the radiation + CNP-18-H mice showed significant decrease in total expiratory time value compared to the sham-irradiated controls from weeks 16–22. The radiation + CNP-18-H mice had obvious less magnitude total expiratory time decrease compared to the radiation-alone group from weeks 16–22. Each value is the mean ± SEM.

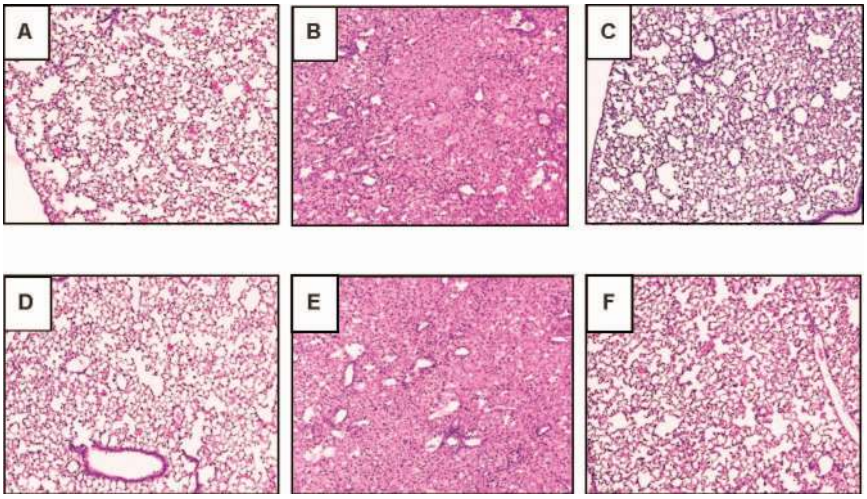

FIG. 4. Representative H&E-stained lung sections show that the CNPs protect lungs from radiation-induced pneumonitis. Lung damage was assessed using H&E staining in sham-irradiated normal lungs (panel A), lungs from radiation-alone mice (panels B and E), lungs from radiation + CNP-18-H mice (panels C and F) and lungs from CNP-18-alone control mice (panel D). The H&E-stained sections from 2 representative mice show significant radiation-induced lung damage in radiation-alone mice (panels B and E). Radiation-induced cell damage was significantly minimized in lungs of 2 representative radiation + CNP-18-H mice (panels C and F). Normal pulmonary architecture is shown in lung sections from both sham-irradiated normal control (panel A) and CNP-18-alone (panel D) mice.

and a significantly lower inflammation score (2.30 ± 0.15) (Fig. 5B, Table 2). The lungs from radiation + CNP-18-H mice had a significant lower vascular damage score (1.73 ± 0.14) compared to that of radiation-alone (2.69 ± 0.19) mice (Fig. 5C, Table 2).

DISCUSSION

The results of this preclinical efficacy study demonstrate that cerium oxide nanoparticle CNP-18, administered as a 10 μ*M* (0.007 mg/kg) IP injection twice a week for 4 weeks starting 2 h after lethal dose WTLI (15 Gy), significantly reduced acute radiation-induced mortality, improved pulmonary function and decreased lung damage in CBA/J female mice (Fig. 2). We used the IP injections based on our previous work, where the biodistribution of CNPs for IP, IV and PO administration routes was compared. Maximum tissue deposition of CNP has been observed with IV injection, whereas minimum CNP tissue deposition has been observed for PO administration. For IP injection, CNP tissue deposition was observed, in the particular order of the spleen > liver > lung > kidney. Therefore, we used IP over IV and PO (*38*). At the study end point of 160 days, 90% of irradiated mice treated with high-dose CNP-18 survived, compared to 10% of mice in the radiation-alone group ($P < 0.0001$) and 30% in the low-dose (100 n*M*) CNP-18 group. Both low- and high-dose CNP-ME-treated irradiated mice showed survival rates (40%, 4/10) that were statistically marginally significant compared to the radiation-alone mice (Fig. 2A, Table 2). The improvement in survival among CNP-18-treated animals correlated with reduced clinical manifestation of disease (Table 2). Lung histology revealed a significant decrease ($P < 0.0001$) in structural damage and collagen deposition in irradiated mice receiving high-dose CNP-18 compared to radiation-alone and low-dose CNP-18-treated mice (Fig. 4). In addition, significant reductions in the inflammatory response ($P < 0.01$) and vascular damage ($P < 0.01$) were observed in the high-dose CNP-18-treated group compared to the radiation-alone control mice (Fig. 5).

Previous attempts to mitigate and treat lung injury as a delayed effect of acute radiation exposure using various free-radical scavengers have had limited success (*8–12*). CNPs have a variety of biological properties that are not found in many other free-radical scavengers. CNPs offer many active sites for free-radical scavenging, their mixed-valence states allow for unique redox chemistry and SOD mimetic activity (*39*) and their free-radical scavenging properties are autoregenerative (*16*). Using CBA/J mice, we provide clear evidence that CNP-18 effectively mitigates radiation-induced lung damage in a dose-dependent fashion with a clearly displayed advantage for the high-dose CNP-18-treated group compared to the low-dose CNP-18-treated group (Fig. 2). Less protection, as observed with CNP-ME treatment, may be due to poor pharmacokinetics or to higher agglomeration and/or different surface chemistry, such as a lower surface Ce^{3+}/Ce^{4+} ratio of CNP-ME (0.45) compared with CNP-18 (1.26) (Table 1). The unique structure of cerium oxide nanoparticles (valence and oxygen defects) promotes cell longevity and decreases toxic insults by virtue of antioxidant effects (*40*), which prevent the accumulation of ROS, thereby preventing the activation of the apoptotic response and cell death.

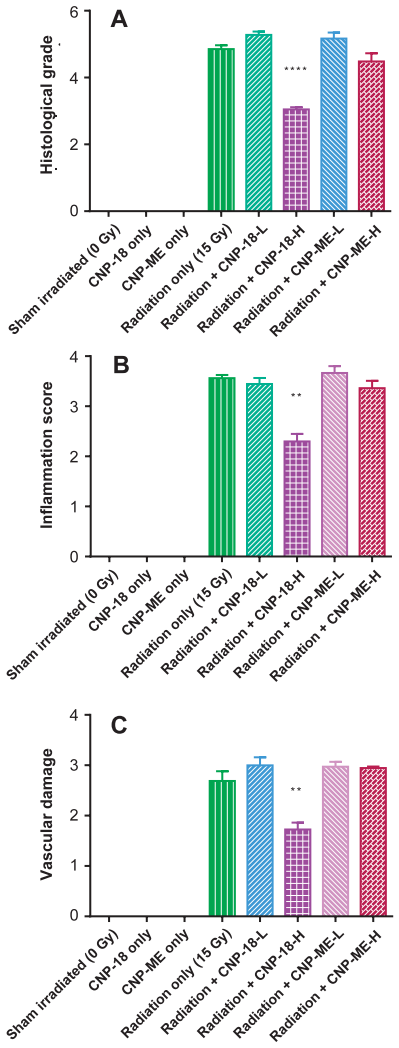

FIG. 5. Semi-quantitative evaluation and scoring of the lung samples. Panel A: Semi-quantitative analysis of lung histology revealed a significant decrease ($P < 0.0001$) in structural damage and collagen deposition in radiation + CNP-18-H mice compared to the radiation-alone group. Panel B: Inflammation scores based on pneumonitis and macrophage invasion. Panel C: Vascular damage score. Each value is the mean ± SEM. $^{****}P < 0.0001$, $^{**}P < 0.01$, radiation + CNP-18-H vs. radiation alone.

The flow ventilated WBP has become widely used to obtain multiple pulmonary measurements on mice without inducing significant injury and distress (*41, 42*). However, there has been considerable concern over its validity, especially for the enhanced pause value (*43, 44*). The WBP studies of lethal dose radiation-induced lung injury in this animal model contribute important longitudinal information to our understanding of radiation-induced lung damage and provide a valuable unbiased end point to evaluate the mitigating efficacy and therapeutic effects of new drugs, compounds, chemicals and biological reagents in murine model platforms. The high-dose CNP-18-treated irradiated mice exhibited significantly lower enhanced pause and pause values than the radiation-alone mice, indicating that high-dose CNP-18 treatment corrected radiation-elevated enhanced pause and pause value and decreased pulmonary distress and bronchoconstriction (Table 3). In addition, multiple respiratory functional parameters suggested possible changes in the amount of airway resistance, which were confirmed by histological findings of airway epithelial cell hyperplasia and fibro-obliteration of the alveoli, all of which result in airflow limitation and impaired gas exchange. Previous studies have shown that enhanced pause is used both as a screening parameter for pulmonary inflammation and as an estimate of airway resistance (*45*), chronic airway inflammation and airway hyperreactivity in mice (*46*), and lipopolysaccharide-induced acute lung injury in rats (*37*).

In conclusion, this preclinical efficacy study demonstrates that CNPs have both clinically and histologically significant mitigating and protective effects on lethal radiation-induced lung injury. Future studies will be conducted to improve the delivery method which may further increase the likelihood of survival after lethal radiation exposures. We will focus on developing an aerosol formulation for direct delivery of CNPs to the lung for a better outcome and to minimize potential side effects. Moreover, the administration of CNPs at delayed time points, such as 24 h or 1–2 weeks postirradiation, will allow us to further evaluate whether CNPs can serve as a practical medical countermeasure (MCM) to mitigate radiation-induced pneumonitis and fibrotic remodeling in the lungs. Finally, additional experiments including systematical analysis of radiation-induced genomic DNA damage, gene transcription and expression changes and epigenetic alterations are warranted to elucidate the mechanism(s) of action of cerium oxide nanoparticles responsible for the radioprotective effects on lethal dose radiation-induced lung injury.

ACKNOWLEDGMENT

This work was supported by the National Institutes of Health, grant no. 1RC1AIO81290-01 (ZV).

Received: September 10, 2015; accepted: March 8, 2016; published online: May 2, 2016

REFERENCES

1. Milano MT, Constine LS, Okunieff P. Normal tissue tolerance dose metrics for radiation therapy of major organs. Semin Radiat Oncol 2007; 17:131–40.
2. Stone HB, McBride WH, Coleman CN. Modifying normal tissue damage postirradiation. Report of a workshop sponsored by the Radiation Research Program, National Cancer Institute, Bethesda, Maryland, September 6–8, 2000. Radiat Res 2002; 157:204–23.
3. Zhao W, Robbins ME. Inflammation and chronic oxidative stress in radiation-induced late normal tissue injury: therapeutic implications. Curr Med Chem 2009; 16:130–43.
4. Trott KR, Herrmann T, Kasper M. Target cells in radiation pneumopathy. Int J Radiat Oncol Biol Phys 2004; 58:463–9.
5. Fleckenstein K, Zgonjanin L, Chen L, Rabani Z, Jackson IL, Thrasher B, et al. Temporal onset of hypoxia and oxidative stress after pulmonary irradiation. Int J Radiat Oncol Biol Phys 2007; 68:196–204.
6. Augustine AD, Gondré-Lewis T, McBride W, Miller L, Pellmar

TC, Rockwell S. Animal models for radiation injury, protection and therapy. Radiat Res 2005; 164:100–9.

7. Riley PA. Free radicals in biology: oxidative stress and the effects of ionizing radiation. Int J Radiat Biol 1994; 65:27–33.
8. Beckman KB, Ames BN. The free radical theory of aging matures. Physiol Rev 1998; 78:547–81.
9. Kaul N, Devaraj S, Jialal I. Alpha-tocopherol and atherosclerosis. Exp Biol Med (Maywood) 2001; 226:5–12.
10. Marchioli R, Schweiger C, Levantesi G, Tavazzi L, Valagussa F. Antioxidant vitamins and prevention of cardiovascular disease: epidemiological and clinical trial data. Lipids 2001; 36:S53–63.
11. Maxwell AJ. Mechanisms of dysfunction of the nitric oxide pathway in vascular diseases. Nitric Oxide 2002; 6:101–24.
12. Meldrum BS. Implications for neuroprotective treatments. Prog Brain Res 2002; 135:487–95.
13. Das S, Dowding JM, Klump KE, McGinnis JF, Self W, Seal S. Cerium oxide nanoparticles: applications and prospects in nanomedicine. Nanomedicine (Lond) 2013; 8:1483–508.
14. Hirst SM, Karakoti AS, Tyler RD, Sriranganathan N, Seal S, Reilly CM. Anti-inflammatory properties of cerium oxide nanoparticles. Small 2009; 5:2848–56.
15. Chen J, Patil S, Seal S, McGinnis JF. Rare earth nanoparticles prevent retinal degeneration induced by intracellular peroxides. Nat Nano 2006; 1:142–50.
16. Das M, Patil S, Bhargava N, Kang JF, Riedel LM, Seal S, et al. Auto-catalytic ceria nanoparticles offer neuroprotection to adult rat spinal cord neurons. Biomaterials 2007; 28:1918–25.
17. Tarnuzzer RW, Colon J, Patil S, Seal S. Vacancy engineered ceria nanostructures for protection from radiation-induced cellular damage. Nano Lett 2005; 5:2573–7.
18. Madero-Visbal RA, Alvarado BE, Colon JF, Baker CH, Wason MS, Isley B, et al. Harnessing nanoparticles to improve toxicity after head and neck radiation. Nanomedicine 2012; 8:1223–31.
19. Wason MS, Colon J, Das S, Seal S, Turkson J, Zhao J, et al. Sensitization of pancreatic cancer cells to radiation by cerium oxide nanoparticle-induced ROS production. Nanomedicine 2013; 9:558–69.
20. Cimini A, D'Angelo B, Das S, Gentile R, Benedetti E, Singh V, et al. Antibody-conjugated PEGylated cerium oxide nanoparticles for specific targeting of Abeta aggregates modulate neuronal survival pathways. Acta Biomater 2012; 8:2056–67.
21. Colon J, Hsieh N, Ferguson A, Kupelian P, Seal S, Jenkins DW, et al. Cerium oxide nanoparticles protect gastrointestinal epithelium from radiation-induced damage by reduction of reactive oxygen species and upregulation of superoxide dismutase 2. Nanomedicine 2010; 6:698–705.
22. Chigurupati S, Mughal MR, Okun E, Das S, Kumar A, McCaffery M, et al. Effects of cerium oxide nanoparticles on the growth of keratinocytes, fibroblasts and vascular endothelial cells in cutaneous wound healing. Biomaterials 2013; 34:2194–201.
23. Das S, Singh S, Dowding JM, Oommen S, Kumar A, Sayle TX, et al. The induction of angiogenesis by cerium oxide nanoparticles through the modulation of oxygen in intracellular environments. Biomaterials 2012; 33:7746–55.
24. Colon J, Herrera L, Smith J, Patil S, Komanski C, Kupelian P, et al. Protection from radiation-induced pneumonitis using cerium oxide nanoparticles. Nanomedicine 2009; 5:225–31.
25. Jackson IL, Xu PT, Hadley C, Katz BP, McGurk R, Down JD, et al. A preclinical rodent model of radiation-induced lung injury for medical countermeasure screening in accordance with the FDA animal rule. Health Phys 2012; 103:463–73.
26. Jackson IL, Xu PT, Nguyen G, Down JD, Johnson CS, Katz BP, et al. Characterization of the dose response relationship for lung injury following acute radiation exposure in three well-established murine strains: developing an interspecies bridge to link animal models with human lung. Health Phys 2014; 106:48–55.
27. Rzigalinski BA, Seal S, Bailey D, Swanand P, inventors. University of Central Florida Research Foundation, Inc., original assignee. Cerium oxide nanoparticles and use in enhancing cell survivability. U.S. patent no. 7534453 B1. May 19, 2009. (bit.ly/226FyL6)
28. Seal S, Karakoti A, inventors. University of Central Florida Research Foundation, Inc., original assignee. Methods and materials for making cerium nanoparticles. U.S. patent no. US20140356271 A1. December 4, 2014. (bit.ly/1q0NJwe)
29. Deshpande S, Patil S, Kuchibhatla SVNT, Seal S. Size dependency variation in lattice parameter and valency states in nanocrystalline cerium oxide. Appl Phys Lett 2005; 87:133113.
30. McGurk R, Hadley C, Jackson IL, Vujaskovic Z. Development and dosimetry of a small animal lung irradiation platform. Health Phys 2012; 103:454–62.
31. Ashcroft T, Simpson JM, Timbrell V. Simple method of estimating severity of pulmonary fibrosis on a numerical scale. J Clin Pathol 1988; 41:467–70.
32. Hübner RH, Gitter W, El Mokhtari NE, Mathiak M, Both M, Bolte H, et al. Standardized quantification of pulmonary fibrosis in histological samples. Biotechniques 2008; 44:507–17.
33. Hoymann HG. Invasive and noninvasive lung function measurements in rodents. J Pharmacol Toxicol Methods 2007;55:16–26.
34. Finotto S, De Sanctis GT, Lehr HA, Herz U, Buerke M, Schipp M, et al. Treatment of allergic airway inflammation and hyperresponsiveness by antisense-induced local blockade of GATA-3 expression. J Exp Med 2001; 193:1247–60.
35. Hantos Z, Brusasco V. Assessment of respiratory mechanics in small animals: the simpler the better? J Appl Physiol (1985) 2002; 93:1196–7.
36. Lomask M. Further exploration of the Penh parameter. Exp Toxicol Pathol 2006; 57 (suppl 2):13–20.
37. Liu F, Li W, Pauluhn J, Trübel H, Wang C. Lipopolysaccharide-induced acute lung injury in rats: comparative assessment of intratracheal instillation and aerosol inhalation. Toxicology 2013; 304:158–66.
38. Hirst SM, Karakoti A, Singh S, Self W, Tyler R, Seal S, Reilly CM. Bio-distribution and in vivo antioxidant effects of cerium oxide nanoparticles in mice. Environ Toxicol 2013; 28:107–18.
39. Heckert EG, Karakoti AS, Seal S, Self WT. The role of cerium redox state in the SOD mimetic activity of nanoceria. Biomaterials 2008; 29:2705–9.
40. Patil S, Sandberg A, Heckert E, Self W, Seal S. Protein adsorption and cellular uptake of cerium oxide nanoparticles as a function of zeta potential. Biomaterials 2007; 28:4600–7.
41. Campbell JD, Buckland KF, McMillan SJ, Kearley J, Oldfield WL, Stern LJ, et al. Peptide immunotherapy in allergic asthma generates IL-10-dependent immunological tolerance associated with linked epitope suppression. J Exp Med 2009; 206:1535–47.
42. Darcan-Nicolaisen Y, Meinicke H, Fels G, Hegend O, Haberland A, Kühl A, et al. Small interfering RNA against transcription factor STAT6 inhibits allergic airway inflammation and hyperreactivity in mice. J Immunol 2009; 182:7501–8.
43. Adler A, Cieslewicz G, Irvin CG. Unrestrained plethysmography is an unreliable measure of airway responsiveness in BALB/c and C57BL/6 mice. J Appl Physiol 2004; 97:286–92.
44. Lundblad LK, Irvin CG, Adler A, Bates JH. A reevaluation of the validity of unrestrained plethysmography in mice. J Appl Physiol 2002; 93:1198–207.
45. Vaickus LJ, Bouchard J, Kim J, Natarajan S, Remick DG. Assessing pulmonary pathology by detailed examination of respiratory function. Am J Pathol 2010; 177:1861–9.
46. Elekes K, Helyes Z, Kereskai L, Sándor K, Pintér E, Pozsgai G, et al. Inhibitory effects of synthetic somatostatin receptor subtype 4 agonists on acute and chronic airway inflammation and hyperreactivity in the mouse. Eur J Pharmacol 2008; 578:313–22.